National Research Council Canada
Conseil national de recherches Canada

Institute for Research in Construction
Institut de recherche en construction

NRCC Air Collector Test Facility: Description, Calibration and Data Manipulation

M.A. Bernier

Internal Report No. 524

Date of issue: March 1987

Canada

ABSTRACT

This report describes the experimental facility used to test air solar collectors at the Institute for Research in Construction (formerly the Division of Building Research) of the National Research Council Canada. It also presents data manipulation and reduction techniques. Finally, the techniques used to calibrate the facility and the calibration are discussed.

NOMENCLATURE

A	Collector aperture area (m^2)
A_t	Orifice plate area (m^2)
C	Discharge coefficient (dimensionless)
C_p	Air specific heat (J/kg•K)
d	Orifice plate diameter (m)
D	Pipe diameter (m)
E	Velocity of approach factor (dimensionless)
G	Global irradiance incident on the collector (W/m^2)
k	Isentropic coefficient (dimensionless)
$\dot{m}_i$	Inlet mass flowrate (kg/s)
$\dot{m}_o$	Outlet mass flowrate (kg/s)
$\dot{m}_{L_o}$	Leakage mass flowrate (kg/s)
P_1	Absolute pressure at the upstream pessure taps (Pa)
P_{in}	Power input to the Calibration Heat Source (W)
P_i	Inlet gauge pressure to the collector (Pa)
P_o	Outlet gauge pressure to the collector (Pa)
Q_c	Collected energy (W)
Re	Reynolds number (dimensionless)
T_1	Absolute temperature at the upstream pressure taps (K)
T_a	Ambient temperature (°C)
T_i	Inlet temperature to the collector (°C)
T_o	Outlet temperature to the collector (°C)
T_L	Air leakage temperature (°C)
T_{L_o}	Air leakage temperature (°C)
T_{sky}	Sky temperature (K)
W	Humidity ratio (kg H_2O/kg dry air)
σ	Stefan-Boltzmann constant ($W/m^2 \cdot K^4$)
ΔP	Pressure different across the orifice plate (Pa)
ΔT	Temperature difference across the collector (K)
η	Thermal efficiency (%)
γ	Gas expansion factor (dimensionless)
ρ_1	Air density at the upstream pressure taps location (kg/m^3)
μ	Air viscosity ($N \cdot s/m^2$)
β	d/D (dimensionless)

1.0 Introduction

The Institute for Research in Construction (formerly the Division of Building Research) of the National Research Council of Canada was involved from 1981 to 1985 in the development of improved thermal performance test

methods and equipment and better characterizations of air solar collectors thermal performance. Thermal performance test methods and characterizations of air solar collectors will be the subject of another paper (1). This report describes the facility used at NRCC to test air collectors. The test facility was bought from the Ontario Research Foundation, who had built similar devices for solar collector commercial testing at the Canadian National Solar Test Facility (2). The facility was modified by NRCC to suit research needs. This note is an account of the hardware and software modifications made to the test facility. As well, a thorough calibration, which is also reported here, was undertaken to minimize experimental uncertainty.

2.0 Description of the facility

2.1 Altazimuth frame

The experimental test facility (Fig. 1) rests on four rubber tire wheels and rotates around two axes (altazimuth tracking). It is anchored to a leveled concrete pad (7 m × 7 m, 1/4° slope allowed for water drainage) via two removable keys (Fig. 2a). With the keys disengaged, the frame can easily be wheeled inside for servicing. Whenver required, an automatic snow melting system is activated to keep the pad free of snow and ice.

A vertical shaft, through a DC motor-worm-gear-chain drive arrangement, provides the azimuth (east-west) rotation. The altitude drive includes two parts: An enclosed worm gear with a DC motor and an open worm gear drive (Fig. 2b). The altitude axle rotates in two pillow block bearings.

Both movements are computer controlled. The computer, using the date and time entered by the operator, positions the altazimuth frame so that the face of the collector is perpendicular to the sun's rays. Potentiometers located on each shaft feed back to the computer the actual position and the computer, by activating the azimuth and /or the altitude drive, makes the necessary adjustments so that the tracking is always within ±1°. These corrections occur approximately once every minute. Limit switches are strategically located on each shaft to prevent over-travel.

2.2 Meteorological measurements

2.2.1 Radiation measurements

The global (beam + diffuse) solar radiation striking the collector is measured using a calibrated Precision Spectral Pyranometer. The PSP is mounted on the tracking altazimuth frame with it's sensing surface coplanar to the collector glazing surface as recommended by ASHRAE Standard 93-77 (3).

The beam component of solar radiation is measured using a calibrated NIP (Normal Incidence Pyrheliometer) mounted on a precise sun tracking device and located on the roof of a nearby building. The amount of diffuse solar radiation received by the collector is not measured; it is simply calculated as the difference between the readings of the PSP and the NIP.

Long wave radiation (thermal sky radiance) is measured using a pyrgeometer. The thermopile voltage output of this instrument is a function of its temperature, which is determined by the balance between absorbed and emitted long wave radiation fluxes. An internal thermistor-battery-resistance circuit produces a voltage proportional to σT^4, where T is the absolute temperature of the instrument. This analog voltage can be added to the thermopile output in order to obtain only the downcoming long wave radiation, σT_{sky}^4, where T_{sky} is the equivalent sky temperature. The pyrgeometer is mounted on the altazimuth frame and its sensing surface is coplanar with the collector surface.

2.2.2 Ambient temperature

The ambient temperature is measured using a five-element silicon temperature sensor encapsulated in a 6 mm stainless-steel tube which is inserted in an aspirated temperature-radiation shield.

2.2.3 Wind speed

Wind speed is measured using a micro response three cup anemometer equipped with a DC generator producing a DC voltage proportional to wind speed. The anemometer is positioned, as recommended by ASHRAE Standard 93-77 (3), at approximately mid-collector height, i.e. 2.4 m above ground, and is mounted on the altazimuth frame (see Fig. 1).

2.3 Air flow circuit

A schematic of the test loop is shown in Fig. 3. The air flow circuit is an open loop. The two-blower configuration permits the variation of inlet pressure and flowrate to the collector. Ambient air enters the circuit at the intake of the inlet blower. Two plug valves located at the discharge of the blower permit the manual control of inlet mass flowrate and pressure. Then the air travels successively from the inlet heater to the upstream orifice plate, to the inlet pressure tape and to the inlet temperature measuring section. The air enters the collector at the bottom, exits at the top where the outlet temperature and pressure are measured, enters the downstream orifice plate section and finally ends up at the suction blower. The outlet mass flowrate is regulated by bleeding air through a computer-controlled bypass.

The piping has a nominal pipe diameter of 100 mm. All of the flexible piping is of the wire-helix type. At the metal-flexible pipe junctions the metal pipe is heavily coated with high vacuum grease before being inserted (approx. 50 mm) into the flex pipe and fastened to it with a hose clamp. The piping is insulated with 20 mm of Armaflex insulation. The Armaflex is painted white to reduce solar gains. Transitions pieces are often required at the inlet and outlet of the collector to go from, for example, a round pipe at the temperature measuring sections to rectangular entrances at the collector inlet (Fig. 2c). The headers, i.e. the pipe sections from the temperature measuring locations to the collector, are insulated with 75 mm of fiberglass pipe insulation and covered with white waterproof tape (Fig. 2d).

2.4 Mass flowrate measurements

Measurements of mass flowrate are made upstream and downstream of the collector using two nominally identical orifice plate sections built according to ASME and ISO procedure (4,5). By selecting one of five orifice plates, collectors can be tested at flowrates up to 0.20 kg/s while maintaining a relatively high pressure drop through the orifices (typically, $\Delta P \approx 1000$ Pa). The calculation procedure as well as construction details of the orifice plate sections are presented in Appendix A.

2.5 Differential temperature measurement

Inlet and outlet temperatures are measured using both silicon transistors and platinum resistance temperature sensors. To obtain the average temperature through the pipe section and decrease the measurement uncertainty, each type of sensor is arranged in an array of five elements connected in series (Fig. 4). Temperature measurement errors due to radiation exchange between the sensors and the duct wall are minimized by insulating the temperature measurement section with 75 mm of fiberglass insulation and by partially shielding each sensor with a stainless-steel tube. The silicon sensors have a negative temperature coefficient and the platinum ones have a positive coefficient, so that an error due to a drift in the computer's A/D converter can be detected as an apparent divergence of the inlet temperature readings.

During collector testing, inlet and outlet temperature measurements are taken at some distance from the actual inlet and outlet of the collector. Even though headers are insulated, heat losses occur. If no correction is applied these losses might introduce a significant systematic error on the temperature difference. Therefore, differential temperature readings are corrected according to the procedure outlined in (6).

2.6 Relative humidity

The relative humidity is measured using a capacitive thin-film humidity sensor. The sensor is located near the intake of the inlet blower and is protected by a small "Stephenson" screen enclosure.

2.7 Inlet and outlet pressure tap sections

The inlet and outlet gauge pressures were measured using a digital micromanometer connected to a piezometer ring (Fig. 2c). The ring, which is similar to the orifice plate piezometer ring, permits the averaging of jthe pressure around the circumference of the pipe. It is preceeded by 0.45 m of straight pipe. Since the inlet and outlet gauge pressures are not measured at the actual inlet and outlet of the collector, a pressure drop test is necessary and correction is applied to obtain the actual inlet and outlet gauge pressures. In the pressure drop test, the collector is removed and both headers are bolted together with a pitot tube inserted at the junction. The fans are then activated and the static pressure drop between the inlet pressure tap and the junction and the pressure drop between the junction and the outlet pressure tap are measured.

2.8 Inlet heater

The air temperature at the collector inlet was controlled within ±0.2°C of the set point by a computer-regulated, multi-element strip heater (9.4 kW).

2.9 Computer

The on-board computer is a Z80A based microcomputer with 38 Kbytes of read-only-memory (ROM) and 26 Kbytes of random access memory (RAM). It has a 16 channel, 12 bit bipolar analog to digital input circuit for data acquisition and a digital output circuit for control. The computer is located inside an instrumentation box (Fig. 2e). It is accessed via a remote terminal located in an office overlooking the test site (Fig. 2f).

2.10 Typical test

Some operations are necessary before actual testing can start, typically the pre-test procedure goes as follows:

1. The collector surface and all radiation measuring instruments are cleaned to remove any dust or dirt accumulation.
2. An opening is made in the loop by unfastening one of the metal-flexible pipe joint to prevent abnormal pressures in the loop as start-up.
3. The two blowers are started. Manual adjustments on the plug valves and on the bypass are made to obtain the required thermal performance test flowrate, as determined by the computer, upstream and downstream of the collector.
4. The metal-flexible pipe joint is refastened.
5. Final adjustments are made on the plug valves and on the bypass so as to obtain the desired inlet flowrate and pressure.

3.0 Data Manipulation

3.1 Data Acquisition

After the pre-test procedures have been completed (Section 2.10) and before the actual testing period, a series of instructions must be sent to the on-board computer in order to inform it of the required thermal performance test conditions. These instructions are performed sequentially after execution has been initiated. Some of the most important commands are described below:

INSTRUCTIONS (in order of execution)	EXPLANATION
$FS_{0.0720}$	Flow Set; sets the inlet flow to 0.0720 kg/s
$TS_{22.0}$	Temperature Set; sets the inlet temperature to 22.0°C

WC — Wait for Control; all further commands are stopped until the inlet temperature, the fluid flowrate and frame azimuth and altitude have reached their set point and maintained it within a certain range for a specified length of time. Typically the following ranges were used:

variable	range	length of time
inlet temp.	±1.0°C	300 sec.
inlet flow	±0.00025 kg/s	300 sec.
tracking accuracy	±1°	10 sec.

WT — After control (WC) has been achieved execution is suspended until the Wait for Time command has elapsed (typically 900 sec). Usually after this "soak" period the temperature rise through the collector is stable.

WS — Wait for Stability: During this period the computer checks (typically every 15 seconds) the peak-to-peak fluctuation of the $(T_i-T_a)/G$ parameter and of the calculated efficiency. If $(T_i-T_a)/G$ remains within 0.003 and the efficiency with 0.03 for a certain period (typically 300 sec.) then stability is achieved and a stable message appears in the data buffering indicating a data point. An audio signal is sent to the operator indicating that stability has been achieved.

SS — A Second Sensor check is performed immediately after WS to check the inlet and differential temperature measured by the secondary temperature sensors (platinum resistance temperature sensor). If the difference between the primary and secondary temperature sensors is greater than 0.2°C the test is stopped and troubleshooting is undertaken to identify the cause of the discrepancy. As well, the outlet flowrate is reported.

MV — After stability has been achieved the MV command is initiated manually by the operator. This command gives the operator the outputs (in millivolts) of every channel. Three of these readings are used later.

Typically during a clear day the collector is tested at one flowrate and three or four (depending on the day's length) inlet temperatures. Table 1 gives an example of a typical on-board computer output. Lines are

printed in memory every 60 seconds. They represent the exponential average* of readings taken every 5 seconds.

After stability has been achieved a Second Sensor check is executed and the result printed in computer memory (again these numbers are exponential averages). Then the MV command is executed and the instantaneous millivolt outputs of every channel are printed. Measurement of long wave radiation (or more precisely T_{sky}) was done, every minute, by a sky independent HP 41-CV based data acquisition system. The beam component of solar radiation was measured and recorded every minute by DBR's liquid collector calorimeter data acquisition system.

3.2 Data Reduction

At the end of the all the raw data, issued from the on-board computer, are transferred to a DEC PDP 11/23 computer. Then a computer program transforms all the raw data into a format compatible with the existing DBR liquid calorimeter data processing software. Briefly, the transformation goes as follows:

1. The raw data file is scanned and the "stable" data points located.
2. The irradiance, ambient temperature, inlet temperature, temperature rise, inlet flowrate and wind speed are averaged over the last five minutes prior to the stable message.
3. The outlet flowrate is "extracted" from the second sensor check.
4. The averaged temperature rise across the collector is corrected for header heat losses.
5. The inlet and outlet pressures and the relative humidity are converted from their millivolt output to engineering units using the appropriate conversion factors.
6. Measurements of T_{sky} and beam radiation are manually merged into the transformed file.

3.3 Data Processing

The data processing software takes a transformed file and calculates values of thermal efficiency (η) and $(T_i - T_a)/G$. The efficiency may be calculated five different ways (1,7):

a) Efficiency based on an enthalpy balance:

i) $\dot{m}_i < \dot{m}_o$ ($P_i < 0$, P_o & 0):

$$\eta = \frac{Q_c}{G \cdot A} = \frac{\dot{m}_o C_p (T_o - T_i) + (\dot{m}_o - \dot{m}_i) C_p (T_i - T_a)}{G \cdot A} \qquad (1)$$

*Exponential averaging:

average measurement at t=60 sec. = $\frac{11}{12}$ (average measurement at t= 55 sec.) + $\frac{1}{12}$ (instantaneous reading at t=60 sec.). Exponential averaging is used to save on-board computer memory.

ii) $\dot{m}_i > \dot{m}_o$ ($P_i > 0$, $P_o > 0$):

$$\eta = \frac{Q_c}{G \cdot A} = \frac{\dot{m}_o C_p (T_o - T_i) + (\dot{m}_i - \dot{m}_o) C_p (T_L - T_i)}{G \cdot A} \qquad (2)$$

where, $T_L = (T_i + T_o)/2$

iii) $P_i > 0$, $P_o < 0$:

$$\eta = \frac{Q_c}{G \cdot A} = \frac{\dot{m}_o C_p (T_o - T_i) + (\dot{m}_o - \dot{m}_i) C_p (T_i - T_a) + \dot{m}_{L_o} C_p (T_{L_o} - T_a)}{G \cdot A} \qquad (3)$$

where, $T_{L_o} = (T_i + T_o)/2$

$\dot{m}_{L_o}$ is estimated by the experimenter (1).

b) Efficiency based on the inlet flowrate:

$$\eta = \frac{Q_c}{G \cdot A} = \frac{\dot{m}_i C_p (T_o - T_i)}{G \cdot A} \qquad (4)$$

c) Efficiency based on the outlet flowrate:

$$\eta = \frac{Q_c}{G \cdot A} = \frac{\dot{m}_o C_p (T_o - T_i)}{G \cdot A} \qquad (5)$$

In these equations the specific heat, C_p, is evaluated using the following algorithm:

$$C_p = [1030.1 - 0.19762\ T + 3.947 \times 10^{-4}\ T^2] \frac{(1 + 1.792\ W)}{(1 + W)}$$

Values of η vs $(T_i - T_a)/G$ can then be plotted. A typical output is presented in Figure 5, where the same data have been plotted three different ways.

4.0 Calibration

Calibration of such a facility is essential to ensure experimental accuracy. In actual fact, an earlier calibration (8) proved to be important as severe inaccuracies were detected. In what follows the measurements have been divided into two categories, critical or non-critical, depending on whether they have a direct or a second order effect on thermal efficiency.

4.1 Calibration of the non-critical measurements

4.1.1 Orifice plate air temperature sensors

Both orifice plate air temperature sensors were calibrated in a temperature bath against a precision platinum resistance temperature sensor that had been calibrated by the Division of Physics of the NRCC. Spot

checks were made at 0°C and 80°C. In every case the sensors were within the accuracy requirement set forward by ASHRAE Standard 93-77 (3), i.e. ±0.5°C).

4.1.2 Wind speed measurement

The manufacturer accuracy claim (±0.1 m/s or 1%) for the wind measurement was deemed sufficient with respect to the ASHRAE Standard 93-77 requirement (±0.8 m/s), therefore, the wind sensor was not calibrated.

4.1.3 Long wave and normal incidence radiation

The pyrgeometer and the NIP were calibrated by Atmospheric Environment Services (AES) in Toronto; no accuracy claims are given with these calibration certificates.

4.1.4 Humidity sensor

The humidity sensor was calibrated by immersing it in saturated salt solutions as recommended by the manufacturer. The results indicate that in the range 0%-75% RH the accuracy is ±2-3% RH, while from 75% to 100% the accuracy is ±5% RH.

4.1.5 Pressure sensors

Calibration of both orifice plate differentials pressure transducers showed that their outputs were within ±1% of the readings given by a Betz manometer (manufacturer accuracy ~ ±0.01 "H_2O).

The barometer used to calculate the barometric pressure was not calibrated as it is a fundamental measurement in itself. The digital micromanometers, used for the measurement of inlet and outlet pressure, were calibrated against a Betz manometer and shown to give readings accurate to ±2% in their range of operation.

4.2 Calibration of the critical measurements

Referring back to Eqns. 1-5, one can see that the measurements of mass flowrate, differential temperature, global irradiance, collector area, air specific heat, ambient temperature and inlet temperature are all critical for an accurate determination of η.

4.2.1 Global solar irradiance

The PSP used to measure global irradiance was calibrated at AES where calibrations are provided to within ±3% of the World Radiation Reference (9).

4.2.2 Collector area

The accuracy of the aperture area measurement, i.e. the area of the collector through which solar radiation is admitted, is typically of the order of ±0005 m^2 (based on random uncertainty of 3 mm on length and width measurements.

4.2.3 Air specific heat

It is estimated that for the temperatures and humidity ratios normally encountered the accuracy of the air specific heat, C_p is ±0.1%.

4.2.4 Ambient temperature

The ambient temperature sensor was calibrated along with the orifice plate air temperature sensors and showed the same accuracy (i.e. ±0.5°C).

4.2.5 Inlet and outlet temperatures

Because the temperature sensors couldn't be immersed in a temperature bath, calibration of the inlet and outlet temperature sensors had to be carried out the following way: The inlet and outlet temperature measuring sections were put end to end and insulated (with approx. 300 mm of fiberglass insulation). A calibrated platinum resistance temperature sensor was inserted in between the two sections and the flowrate was set to 0.10 kg/s. In this way the output of the inlet and outlet temperature sensor could be checked against the calibrated sensor. Results of the calibration are presented in Table 2.

It can be seen that the primary and secondary sensor readings are within the ASHRAE (3) accuracy envelope of ±0.5°C.

4.2.6 Mass flow rate and differential temperature measurements

The secondary measurements needed in the determination of the mass flowrate, i.e. the barometric pressure, the orifice plate air temperatures, the differential pressure and the humidity measurements were all calibrated (see above).

Calibration of the $\dot{m}$ measurement per se, which would include the errors in the secondary measurements as well as errors inherent to the design of the orifice plate, was not undertaken due to the difficulty in finding a good flowrate measurement against which both $\dot{m}$ could be calibrated. Also, as mentioned above, the differential temperature measurement could not be calibrated individually. For these two reasons an overall calibration of the Q_c measurement (which includes the measurement error on $\dot{m}$, C_p and on ΔT) was performed.

Briefly, in the overall calibration approach (8), the solar collector is replaced with a Calibration Heat Source (CHS) (10), which transfers an accurately measured quantity of electrical energy, P_{in}, to the circulating fluid (air). Assuming zero leakage* in the CHS, and knowing that the amount of energy collected, Q_c, can be expressed as:

$$Q_c = \dot{m}_i \cdot C_p \cdot \Delta T = \dot{m}_o \cdot C_p \cdot \Delta T$$

*A static leakage test was performed on the CHS and the leakage rate was found to be 5×10^{-5} kg/s @ -1000 Pa of pressure, thus leakage is considered negligible.

The accuracy can the be determined by comparing Q_c as measured by the test loop (including it's software processing), with the known power input P_{in}. Calibrations were performed on all five orifice plates with the inlet temperature equal to the ambient temperature (Table 3) and with one orifice plate (orifice plate B) at $T_i > T_a$ (Table 4). The accuracy of Q_c is defined as:

$$\frac{P_{in} - Q_c}{P_{in}} \times 100$$

It is relatively safe to say, based on these results that the accuracy on the Q_c measurement is ±1.5%.

Table 5 summarizes the calibration results of the critical measurements. A detailed uncertainty analysis of air solar collector test results is presented in (1).

5.0 Conclusion

This paper described the experimental test facility used to test air solar collectors at the NRCC. Results of a thorough calibration of the facility indicates that the amount of energy collected can be measured to an accuracy of ±1.5% in the range of flowrates and temperatures normally encountered in air collector testing.

Acknowledgement

The author would like to express his gratitude to Mr. L.P. Chabot who helped in modifying and calibrating the facility.

References

1. Bernier, M.A., Plett, E.G., On Thermal Performance Representation and Testing of Air Solar Collectors. In preparation.

2. Outdoor Solar Collector Test Equipment at the National Solar Test Facility, Ontario Research Foundation, Report No. PHYS. G.P. 81-15, 1981.

3. Methods of Testing to Determine the Thermal Performance of Solar Collectors, American Society for Heating, Refrigerating and Air-Conditioning Engineers, ASHRAE Standard 93-77, 1977.

4. Fluid Meters, Their Theory and Application, American Society of Mechanical Engineers, Fifth Edition, New York, 1959.

5. Measurements of Fluid Flow by Means of Orifices Plates, Nozzles and Venturi Tubes Inserted in Circular Cross-Section Conduits Running Full, ISO Standard 5167-1980(E), ISO Standards Handbook 14, 1983.

6. Bernier, M.A., Correcting for Header Heat Losses when Testing Solar Collectrors, ISES World Congress, Montreal, June 1985.

7. Bernier, M.A., Thermal Performance Representation and Testing of Air Solar Collectors, M.Eng. Thesis, Carleton University, Ottawa, 1985.

8. Bernier, M.A., NRCC Air Collector Test Facility, First EC conference on Solar Heating, Amsterdam, Netherlands, 1984, pp. 499-503.

9. Hay, J.E., Wardle, D.I., An Assessment of the Uncertainty in Measurements of Solar Radiation, Solar Energy, Vol. 29, No. 4, 1982, pp. 271-278.

10. Wright, J.L., Hollands K.G.T., A Calibration Collector for Solar Air Heater Test Loops, University of Waterloo Research Institute, Final Report for DSS contract 07SU.31155-0-2605, Waterloo, 1980.

11. Sodec, F., Moog, W., Influence of Friction on the temperature of a flowing gas, Ki (Klima-und Kaelteingenieur) 1(7), 23-26, 1973. (Translated from German to English by the Canadian Institute for Scientific and Technical Information).

12. Procedure for determining Heat and Cooling Loads for Computerizing Energy Calculations - Algorithms for building heat transfer subroutines, ASHRAE, 1976.

Table 1. Typical on-board computer output

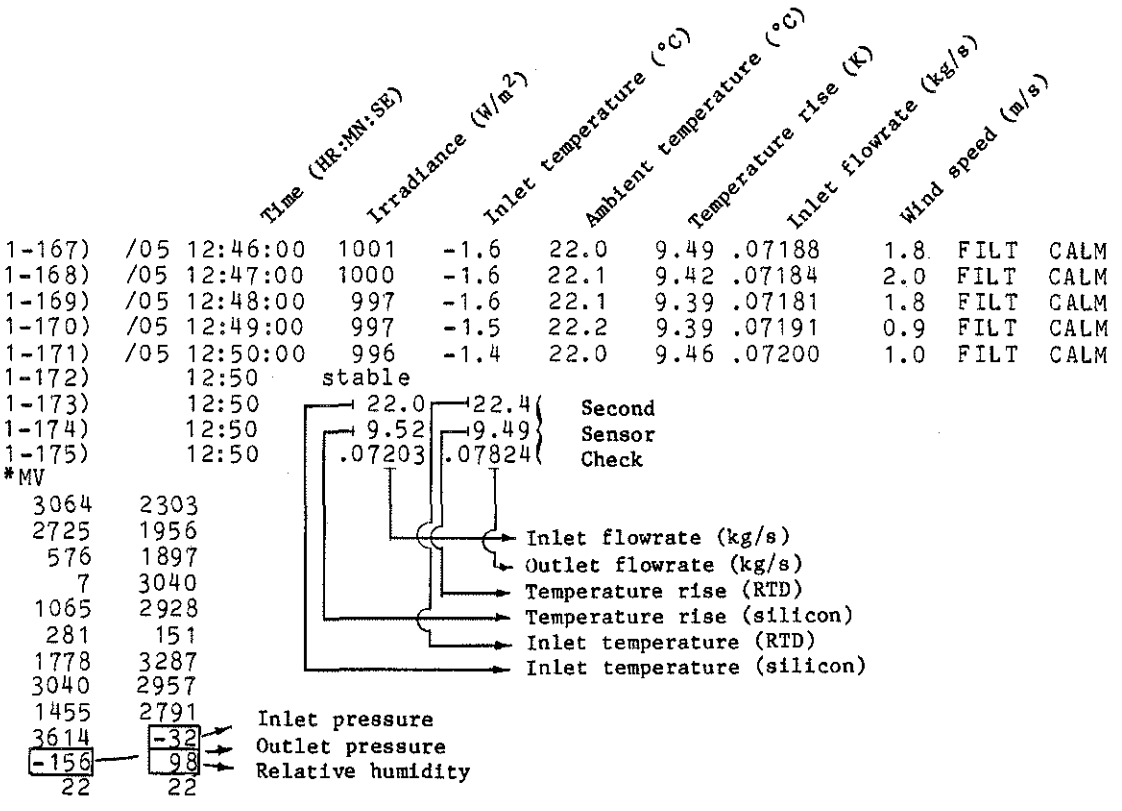

Table 2. Calibration of the inlet and outlet temperature sensors

	T_1		T_o	
(calibrated sensor)	Primary sensor	Secondary sensor	Primary sensor	Secondary sensor
25.3°C	25.5°C	25.5°C	25.5°C	25.5°C
77.6°C	77.8°C	77.2°C	77.7°C	77.1°C

Table 3. Calibration of the Q_c measurement ($T_i = T_a$ in all cases)

Flowrate inlet (kg/s)	Flowrate outlet (kg/s)	Orifice	P_{in} (W)	Accuracy of Q_c ($\dot{m}_i$) (%)	Accuracy of Q_c ($\dot{m}_o$) (%)
0.0151	0.0151	E	498	+ 0.1	- 0.2
0.0252	0.0253	D	1006	+ 0.1	- 0.4
0.0456	0.0457	C	1005	+ 0.1	- 0.3
0.0807	0.0812	B	1002	- 0.8	- 1.3
0.1597	0.1599	A	1005	+ 1.4	+ 1.3

Table 4. Calibration of the Q_c measurement $T_1 > T_a$ (T_a = 25°C and orifice plate B in all cases)

Flowrate inlet (kg/s)	Flowrate outlet (kg/s)	T_i (°C)	P_{in} (W)	Accuracy of Q_c ($\dot{m}_i$) (%)	Accuracy of Q_c ($\dot{m}_o$) (%)
0.0807	0.0812	26.0	1002	- 0.8	- 1.3
0.0808	0.0814	35.0	993	- 0.2	- 1.0
0.0808	0.0813	44.9	973	- 0.7	- 1.3
0.0808	0.0812	54.9	962	- 0.3	- 0.8

Table 5. Accuracy on individual measurements

Measurement	Accuracy
$\dot{m}_i C_p (T_o - T_i)$	± 1.5%
$\dot{m}_o C_p (T_o - T_i)$	± 1.5%
T_i	± 0.5°C
T_a	± 0.5°C
G	± 3%
A	± 0.005 m^2

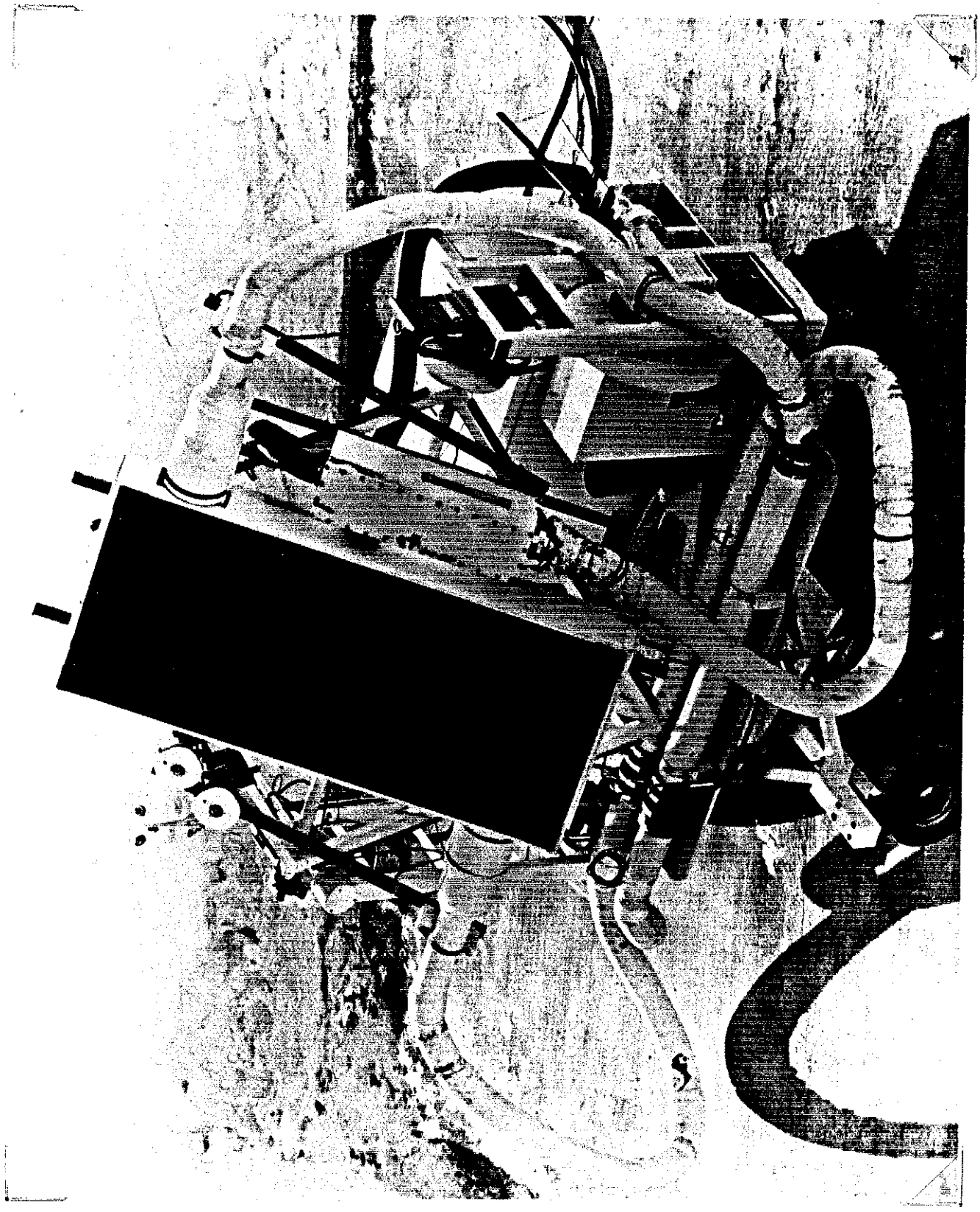

Figure 1. NRCC air solar collector test facility

a) Azimuth drive

b) Altitude drive

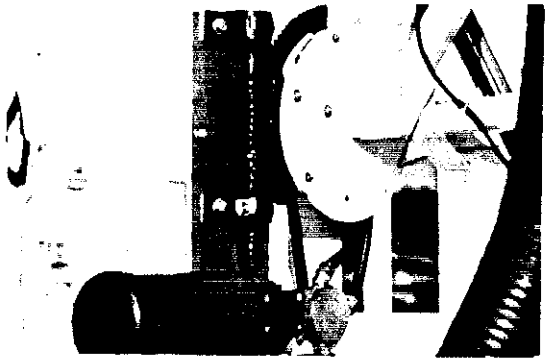

c) Inlet header (uninsulated)

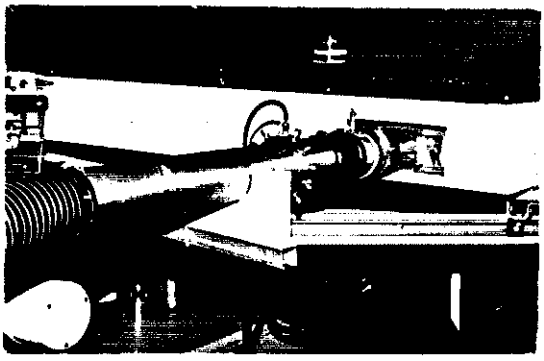

d) Inlet header (insulated)

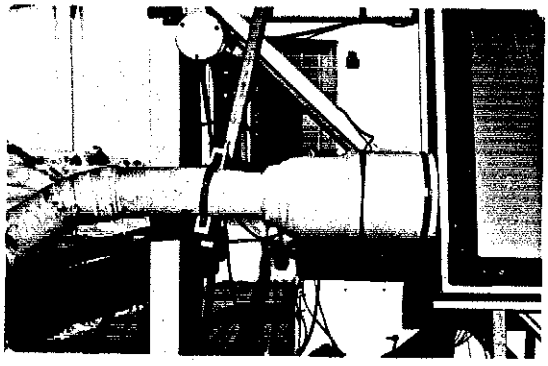

e) Instrumentation box

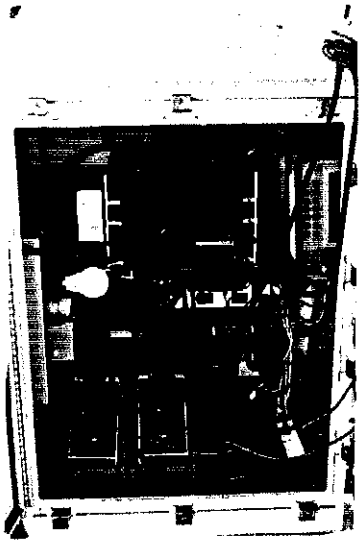

f) Remote control operation

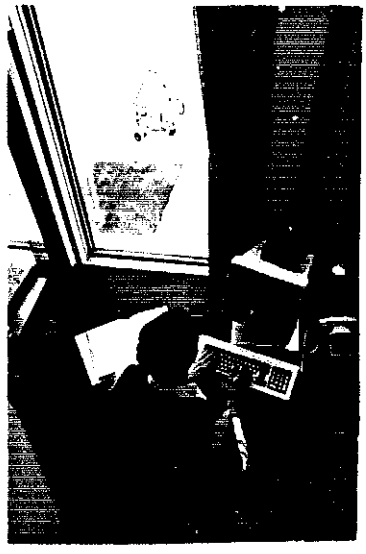

Figure 2. Solar collector test facility - individual components

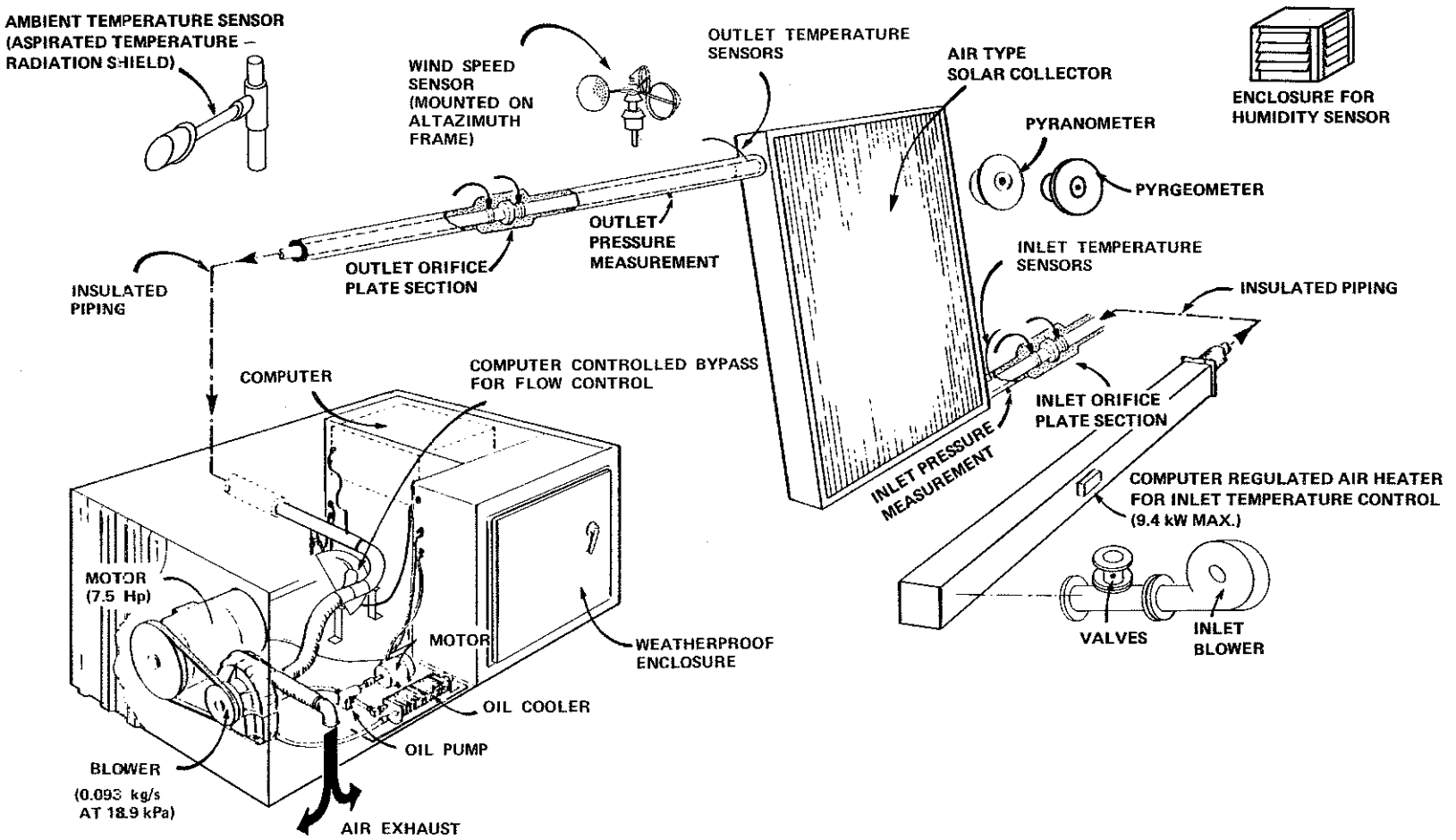

Figure 3. Air flow circuit - air solar collector test facility

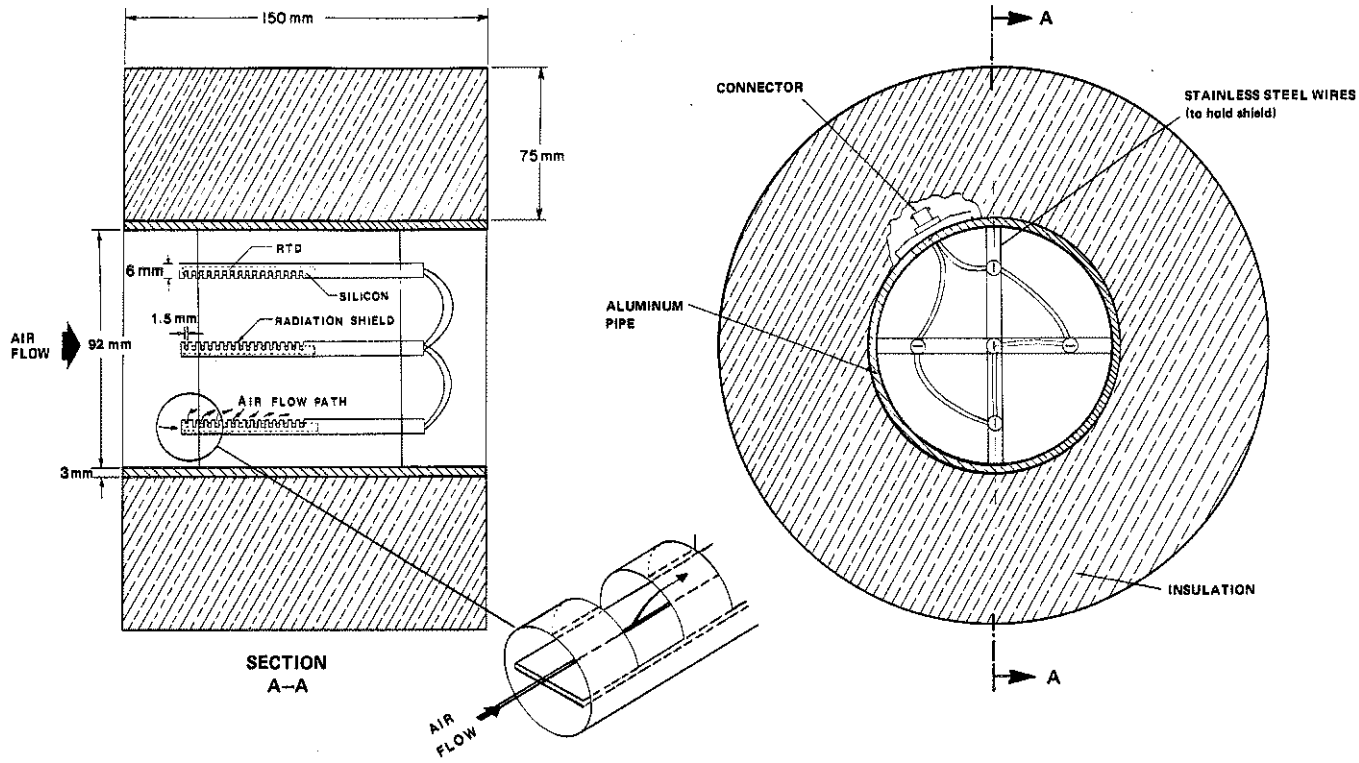

Figure 4. Temperature measuring section

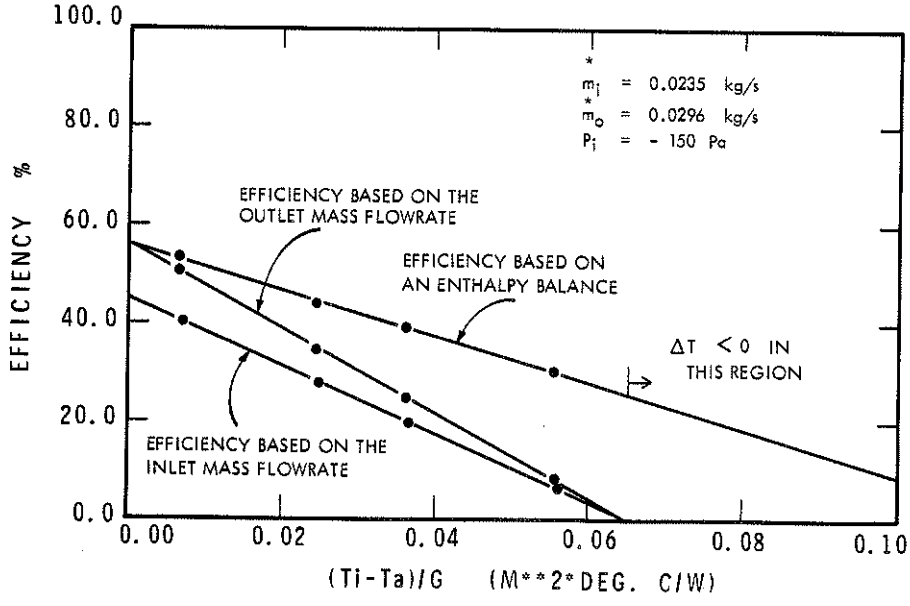

Figure 5. Data plotted by three different methods (inward leakage case)

APPENDIX A
The Measurement of Air Mass Flowrate Using Orifice Plates

1.0 Principle of the method

A primary device, the orifice plate, is inserted in a pipe in which a fluid is running full. The static pressure difference created by the introduction of the primary device is measured by secondary devices (manometer, pressure transducer) and the AIR mass flowrate can be determined according to the following equation (in S.I. Units):

$$\dot{m} = C \cdot E \cdot \gamma \cdot A_t \cdot [2 \cdot \Delta P \cdot \rho_1]^{\frac{1}{2}}$$

where,

$\dot{m}$ is the air mass flowrate (kg/s)
C is the discharge coefficient (dimensionless):

$$C = 0.5959 + 0.0312\ \beta^{2.1} - 0.1840\ \beta^{8} + 01.71\ \beta^{2.5} Re^{-0.75} + (0.0390\ \beta^{4})/(1-\beta^{4}) - 0.01584\ \beta^{3}$$

E is the velocity of approach factor (dimensionless):

$$E = (1-\beta^{4})^{-0.5}$$

γ is the gas expansion factor (dimensionless), for orifice plates:

$$\gamma = 1 - (0.41 + 0.5\ \beta^{4})\ 0 \frac{\Delta P}{k \cdot P_1}$$

A_t is the orifice area (m^2)
ΔP is the differential pressure across the orifice (Pa)
ρ_1 is the air density in the plane of the upstream pressure taps (kg/m^3). For an air-water vapor mixture, ρ_1 may be expressed as:

$$\rho_1 = 0.0034858 \frac{P_1\ (1 + W)}{T_1\ (1 + 1.608\ W)} \text{ (for } P_1 \text{ near atmospheric pressure)}$$

P_1 is the absolute pressure at the upstream pressure taps (Pa)
T_1 is the absolute temperature in the plane of the upstream pressure taps, K
W is the humidity ratio, kg H_2O/kg dry air
Re is the Reynolds Number (dimensionless)

$$Re = \frac{4 \cdot \dot{m}}{\mu \cdot \pi \cdot D}$$

μ is the air viscosity ($N \cdot s/m^2$)
k is the isentropic coefficient (k=1.4 for air)
β = d/D
d is the orifice diameter (m)
D is the upstream internal pipe diameter (m)

2.0 Note on the evaluation of C

The discharge coefficient, C, is a function of $\dot{m}$, the mass flowrate. The mass flowrate being unknown at the start, an interative process has to take place: A flowrate is guessed and an estimate of C obtained, with this estimate of C a new $\dot{m}$ is calculated and the process is repeated until convergence is obtained (usually 3-4 iterations).

3.0 Construction details

The two identical orifice plate sections were built according to ISO and ASME (4,5) specifications (Figs. A1 and A2). The orifice plate sections are made of brass as it was the only material meeting the circularity and roughness of pipe requirements. The orifice plates are made of stainless-steel. The tolerances set forward in (5) for the perpendicularity of the orifice plate, the pressure tapping arrangement and the required straight length of pipe before and after the plates were all surpassed. After construction, both orifice plate sections were sealed at both ends and pressurized to approximately 35 kPa; no leaks were detected.

4.0 ΔP, $\rho_1(P_1, T_1, W)$ measurements

The static pressure drop across the orifice, ΔP, is measured using a variable reluctance pressure transducer. The determination of the density, ρ_1, requires the measurement of P_1, T_1, W. The absolute pressure at the upstream pressure tap, P_1, is obtained by subtracting from the local barometric pressure measurement the pressure difference, as measured by a digital micromanometer, from ambient to the upstream pressure tap. The air temperature, T_1, is measured using five elements silicon temperature sensors, located 530 mm downstream from the upstream pressure taps. The humidity ratio, W, is obtained from the relative humidity (section 2.6) and ambient temperature measurements (section 2.2.2) using the algorithm described in (12).

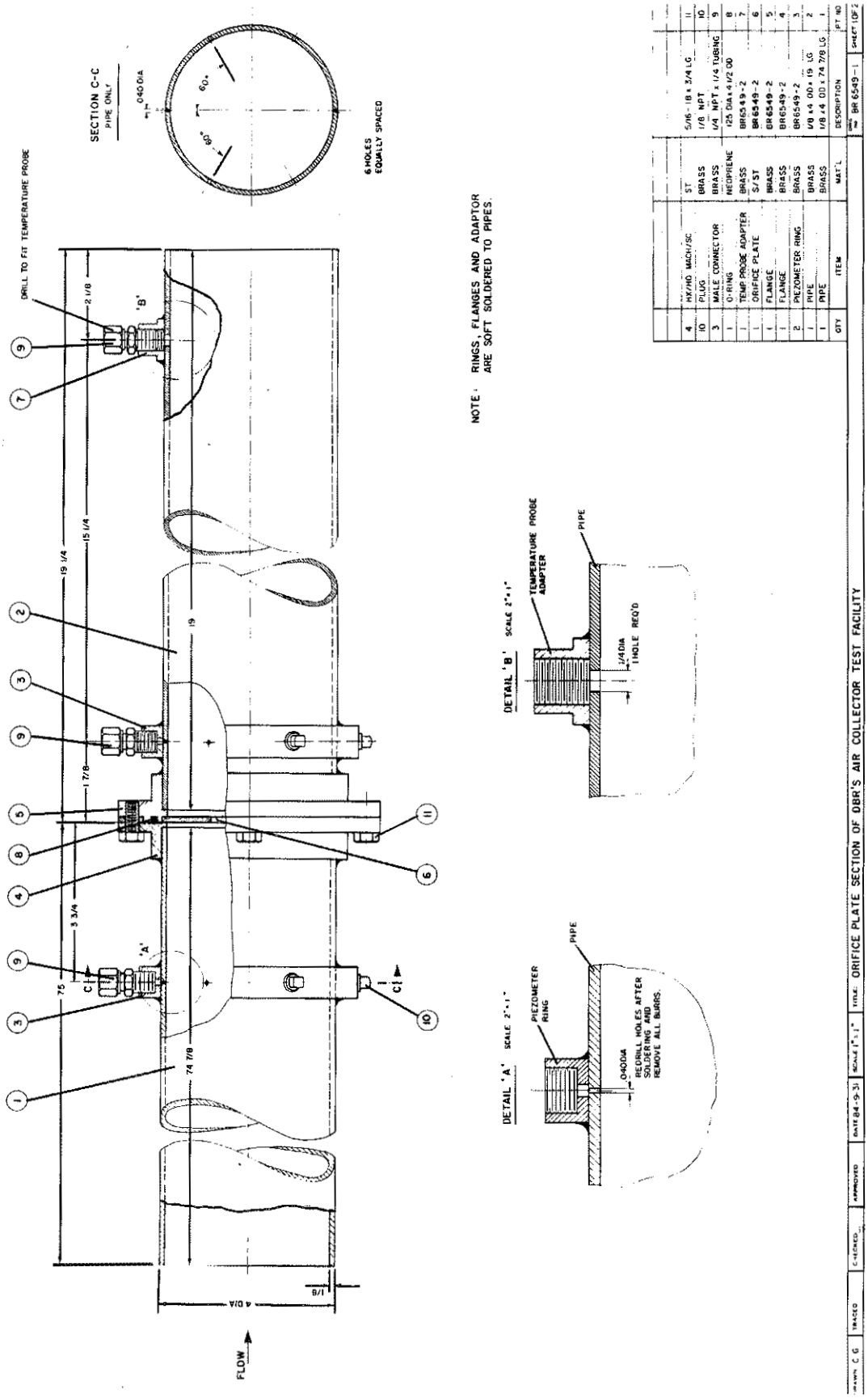

Figure A1. Orifice plate section - air collector test facility

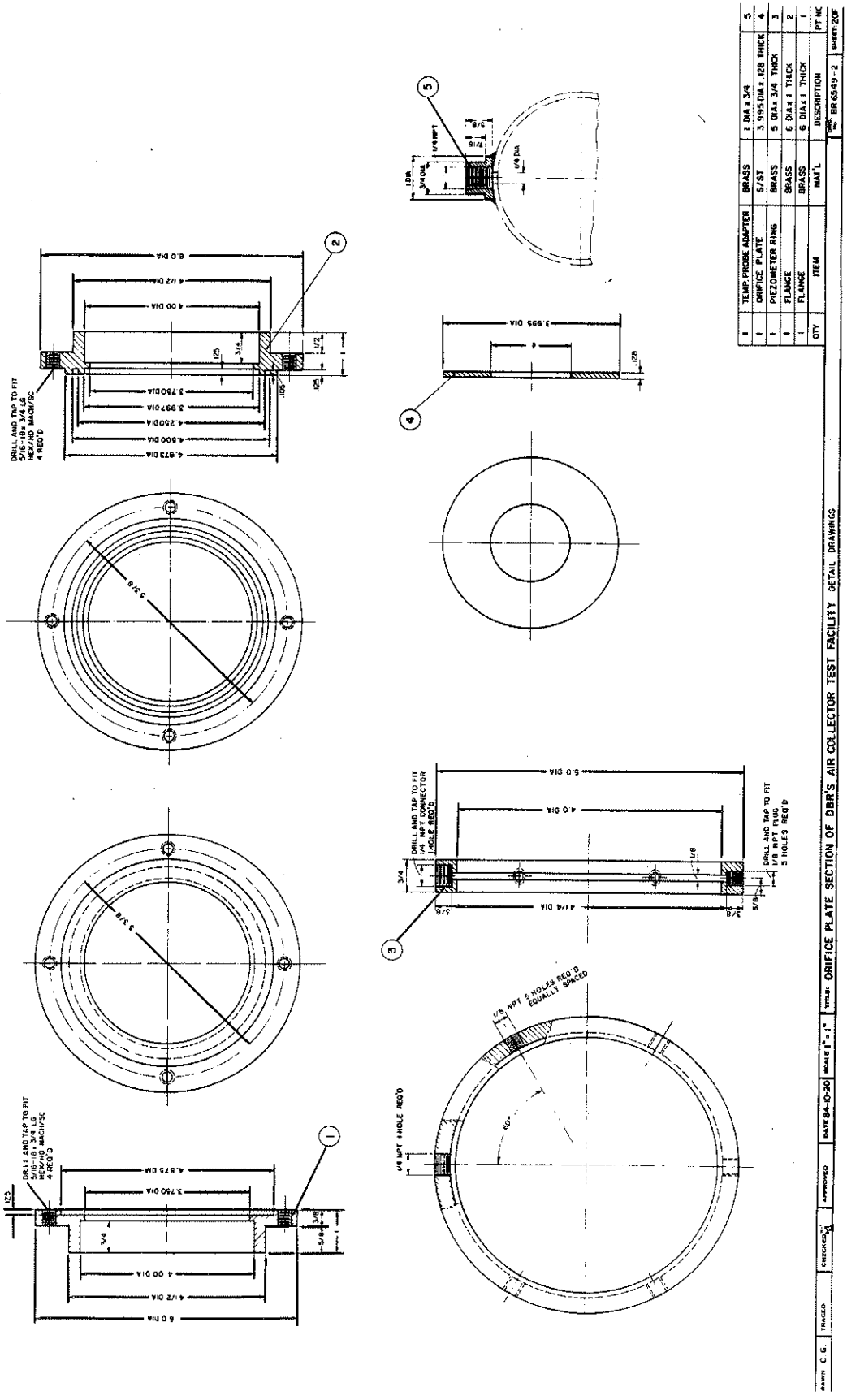

Figure A2. Orifice plate section - air collector test facility (detail)